Solar Energy Materials and Solar Cells 202 (2019) 110126

Contents lists available at ScienceDirect

Solar Energy Materials and Solar Cells

journal homepage: www.elsevier.com/locate/solmat

Theoretical insights into the stability of perovskite clusters by studying water adsorption on $(CH_3NH_3)_4SnI_6$

Zhengyang Gao[a,*], Ge Yan[a], Mingliang Zhao[a], Shaopeng Xu[a], Linlin Li[a], Hanyu Huang[a], Weijie Yang[a,**], Xunlei Ding[b]

[a] School of Energy and Power Engineering, North China Electric Power University, Baoding, 071003, China
[b] School of Mathematics and Physics, North China Electric Power University, Beijing, 102206, China

ARTICLE INFO

Keywords:
Perovskite solar cells
Water molecules
Adsorption
Density functional theory

ABSTRACT

Perovskite solar cells have great development prospects due to their high photoelectric conversion efficiency and low cost. However, perovskite materials are easy to decompose under water conditions, directly reducing the efficiency of perovskite solar cells. Cluster model was applied to study the mechanism of the effect of water on perovskite materials. Density functional theory has carried on to theoretically calculate the structure and energy of perovskite cluster after adsorbing water molecules. The usage of independent gradient model (IGM) showed the interaction region between perovskite cluster and water molecules. The bonding types between atoms were qualitatively obtained by analysis of atoms in molecules (AIM), and the microscopic mechanism of interaction between perovskite cluster and water molecules is revealed. The results show that when the number of the interactions between perovskite cluster and water molecules increases, the stability of the adsorption configuration will enhance. The interaction type between perovskite cluster and water molecules belongs to hydrogen bond and it also affects the stability of the perovskite cluster. This result can contribute to understand the stability of perovskite clusters by studying water adsorption on $(CH_3NH_3)_4SnI_6$ and to furtherly improve the practicability of perovskite solar cells.

1. Introduction

Perovskite solar cells (PSCs) have attracted extensive concentration from scholars since they were proposed in 2009 [1], and were rated as one of the top ten scientific breakthroughs in 2013 [2,3]. In the 1960s, Shockley and Queisser [4] put forward the theory of the efficiency limit of semiconductor photovoltaic solar cells based on the detailed balance analysis of photovoltaic physical processes. Now, the efficiency of silicon solar cells, as traditional solar cells, is close to 25% [5], which is quite close to the limit of his theoretical calculation. Hybrid organometallic perovskite (HOP) as absorbers, such as $CH_3NH_3PbI_3$, proved to be a standard direct band-gap semiconductor with a bandwidth of nearly 1.5 eV and a fairly strong adsorption coefficient for visible and near-infrared parts of the solar spectrum [6]. JE Spanier et al. [7] used the ferroelectric insulator $BaTiO_3$ to show how photogeneration and the collection of hot non-equilibrium electrons through the bulk photovoltaic effect yields a greater-than-unity quantum efficiency. This device breaks through the efficiency predicted by Shockley-Queisser limit of this bandgap. HOP is also ferroelectric, which may has similar situation with $BaTiO_3$ and may give rise to conditions for breaking through Shockley's theory. Comparing with silicon solar cells, the preparation process of PSCs is simple and have obvious advantages in thickness, which can significantly reduce the manufacturing cost of solar cells [8]. Thin film solar cells mainly include GaAs, InP, CIGS, CdTe. This kind of solar cells has high photoelectric conversion efficiency and low consumption of raw materials, but some material elements used in the solar cells are toxic or scarce, which limits its wide use in a large area. PSCs have developed very rapidly in recent years. The photoelectric conversion efficiency of perovskite solar cells was only 3.8% [1] in 2009. In 2013, Im et al. manufactured $CH_3NH_3PbI_3$ nanocrystals. The efficiency of this materials used for photoelectric conversion reached 6.5% [9]. From 2014 to 2018, the efficiency of perovskite solar cells had reached from 13.9% to 23.2% [10–12]. In 2019, KRICT scientists have prepared a new perovskite material, which has set a new record of 24.2% [13]. The perovskite solar cells developed from single-junction to two-junction structures over the past

* Corresponding author.
** Corresponding author.
E-mail addresses: gaozhyan@163.com (Z. Gao), yange1213@163.com (G. Yan), zhaoml2510@ncepu.edu.cn (M. Zhao), xsp.ncepu@outlook.com (S. Xu), SDUTLL@163.com (L. Li), 13933114556@163.com (H. Huang), yangwj@ncepu.edu.cn (W. Yang), dingxl@ncepu.edu.cn (X. Ding).

https://doi.org/10.1016/j.solmat.2019.110126
Received 26 June 2019; Received in revised form 11 August 2019; Accepted 13 August 2019
Available online 29 August 2019
0927-0248/

decade. In 2018, Oxford PV company declared the perovskite/silicon tandem solar cell with a 28% conversion efficiency, which is outstanding than perovskite and silicon solar cells. Building-integrated photovoltaics is another promising application. Saule Technologies has applied semi-transparent perovskite photovoltaic devices into an office building preferentially. Other perovskite-based applications, such as light-emitting diodes, detectors and photocatalysts, samely have tremendous potential [14]. The photoelectric conversion efficiency of perovskite solar cells is expected to be further improved so it has great application prospect for development [15].

Stability of materials is a key issue in solar cells design, prepation and application, which may greatly influence effectiveness and cost of solar cells [16,17]. Stability is the most lethal weakness of perovskite solar cells especially when water acts on them. Due to the instability of perovskite materials, the use of perovskite solar cells in real society is seriously restricted, and the research on its stability is gradually increasing. De Wolf et al. [18] researched the moisture induced decomposition of $CH_3NH_3PbI_3$ and reported that a two orders of magnitude reduction of the adsorption in the range from 1.5 to 2.5 eV would happen when exposuring to humidity for 20 h. Frost et al. [19] showed that $MAPbI_3$ would bind with a water molecule, and a proton in the methylamine ion would be captured, and finally decomposed into a hydrate of methylamine and HI. It was inferred that replacing the organic ions of perovskite with proton-free ion groups, such as $(CH_3)_4N^+$, would improve the stability of perovskite. Jiang et al. [20] replaced two iodine ions in with two haloid thiocyanate ions. $CH_3NH_3Pb(SCN)_2I$ was placed in 95% humidity for 4 h and no degradation of it was observed. But obvious degradation was oocurs in $CH_3NH_3PbI_3$ under the same conditions. The results showed that the humidity stability of this new perovskite material $CH_3NH_3Pb(SCN)_2I$ was much higher than the traditional perovskite $CH_3NH_3PbI_3$. Thus, the stability of hybrid perovskite can be improved by adjusting the composition of perovskite materials and finding suitable combinations without affecting the efficiency. According to our assumption, firstly the size of perovskite clusters can be increased or decreased to study the effect of cluster size on the adsorption of water molecules by perovskite clusters. Secondly, Sn^{2+} and I^- can be replaced to study the effect of inorganic element on water molecules adsorbed by perovskite clusters. Finally, $CH_3NH_3{}^+$ can be replaced to study the effect of organic elements.

Comparing with periodic model, the cluster model can be reliable and more suitable to be applied to research the stability of perovskite. The changes of cluster size, from small clusters including a few atoms to large clusters including tens of thousands of atoms, provides a distinctive way to feature and to control the bulk properties [21]. Li et al. [22] studied the additive coordination effect on hybrids perovskite crystallization and opened a new direction on the film formation study. Another important use of clusters is to accurately analyze the relationship between structure and activity [23]. Cluster model is reliable and able to obtain accurate results. The electronic wavefunctions about the cluster models have advantages of understanding the local properties of condensate [24]. The cluster wavefunctions, acquired from molecular orbital theory, are able to relate chemical conception developed to describing molecular chemical bonds to the chemical bonding at the surface and in the bulk of condensate [25]. Giacomo Giorgi et al. [26,27] established the perovskite cluster model of mixed organic-inorganic halide which chemical formula was $(MA)_jPb_kX_l(l = j + 2k)$; MA is methylammonium and X is halogen). The structure of the specific cluster model at k = 1, 2, 8 and 12 was calculated, and the energy decomposition and charge density analysis were carried out. The results show that there is a certain relationship between the total dielectric dipole moment and the spatial distribution of the wave function of the molecular orbital. Although the electronic and optical properties of three-dimensional or two-dimensional perovskite have been studied extensively in recent years [28–32], few articles have been published to study the structure and properties of 0-dimensional perovskite at atomic scale.

The first principles, as the basic calculation mechanism, which refers to the self-consistent calculation of the atomic composition of the materials studied by means of quantum mechanics. It introduced three basic approximations: Born-Oppenheimer approximation,Hatree-Fock self consistent field method, Kohn-Sham equation. And the most commonly used method of the core step in first-principles calculation is density functional theory (DFT). It should be underlined that the complex interactions and the various spatial, temporal, and energy scales present in multi-component systems make the description of these processes a relatively difficult task. But it cannot be denied that theoretical calculation could help in studying the adsorption mechanism and assisting the subsequent experimental research and design of practical application.

Due to the blank research on the stability of perovskite clusters influenced by water factors, the microscopic mechanism of perovskite clusters adsorbing water molecules has aroused our interest. From the water adsorption by perovskite clusters, the size and type of interactions between them was studied and the structural stability of perovskite before and after adsorption was analyzed. In this work, the micromechanism of perovskite clusters adsorbing water molecules was researched at molecular level. Firstly, density functional theory calculations were used to research the structure and energy of perovskite clusters adsorbing water molecules. Secondly, it is necessary to investigate the interaction region between perovskite cluster and water molecules through using IGM analytical methods. Thirdly, the bonding types between atoms were obtained by AIM topological analysis qualitatively. Ultimately, the microscopic mechanism of interaction between water molecules and perovskite cluster was analyzed from these works. This work can provide a more deep and systematic understanding of the perovskite cluster adsorbing water molecules so as to obtain innovative breakthroughs on the stability of PSCs and has guiding significance on the commercialization and practical applications for PSCs.

2. Computational methods

According to the model from Giacomo Giorgi [33], the Gaussian 09 software package [34] was used to construct the perovskite cluster model, and the structure was optimized to obtain the structure with the lowest energy. All the calculations including structural optimization and energy calculation were carried out by ORCA 3.0.1 [35] software. Specifically, structural optimization used BLYP density functional method [36] and def2-SVP basic set [37], and the more accurate def2-QZVP basic set [37] was used for energy calculation. Grimme's DFT-D3(BJ) method was used for correction of dispersion interaction using Becke-Johnson damping function [38] and BLYP-D3 functional was selected for the ability to research the interaction between large systems [39]. It can obtain favorable results for non-covalent interactions with saving computing resources. Today almost all mainstream quantization programs support DFT-D3 [40–44]. Grimme's gCP [45] method was used to obtain correction energy of Basis Set Superposition Error (BSSE). In order to speed up the calculation, RI technique [46] was used for accelerating self-consistent field (SCF), and accuracy deviation due to RI technique is negligible [47]. From this, 9 different adsorption configurations were obtained respectively.

The IGM isosurface of adsorption configuration was obtained by using wave function analysis software Multiwfn 3.6 [48]and visualization program VMD 1.9.1 [49] in order to visualize the region and type of weak interaction. On the basis of AIM theory [50], topological structure of the electron density distribution function was performed, bonding types and strength between atoms were quantitatively analyzed, and it was also explored that how the amount of water molecules influence the perovskite cluster adsorbing water molecules.

The adsorption energies of perovskite cluster after adsorbing water molecules were calculated as follows [51]:

$$\Delta E_{ads} = \left[E_{surf+nH_2O} - E_{surf} - nE(H_2O)\right]/n \quad (1)$$

Where E_{surf} and E_{H_2O} represent the energy of perovskite molecule and water molecule respectively, $E_{surf+nH_2O}$ is the energy of perovskite clusters after adsorbing n water molecules. If the absolute value of adsorption energy is 0–40 kJ mol^{-1}, the adsorption is weak and belongs to physisorption. If the absolute value of adsorption energy is more than 50 kJ mol^{-1}, the adsorption is strong and belongs to chemisorption [52].

3. Results and discussions

3.1. Perovskite cluster modeling

The general chemical formula for perovskite is ABX_3. Goldschmidt [53] proposed the tolerance factor t to describe the relationship between the structural stability of perovskite and the ion radius, shown as follows:

$$t = \frac{R_A + R_X}{\sqrt{2}(R_B + R_X)} \quad (2)$$

In the formula, R_A, R_B, R_X represents the radius of A, B and X ions in ABX_3.

The value of $(CH_3NH_3)_4SnI_6$ is 0.852 (R_A = 0.180 nm, R_B = 0.112 nm, R_X = 0.220 nm), which means the formation of $(CH_3NH_3)_4SnI_6$ is possible. Therefore, the formation of $(CH_3NH_3)_4SnI_6$ studied in this paper is possible. Besides, studying the lead-free perovskite with low-toxicity, narrow optical bandgap, high charge carrier mobility would be a meaningful matter. Hence, Sn-based perovskite material was selected as the research object.

Perovskite cluster can be expressed by molecular formula $(MA)_j M_k X_l$ $(l = j + 2k)$. The structure selected in this study is $(CH_3NH_3)_4SnI_6$ when j equals 4. The lowest energy structure after optimizing is shown in the following Fig. 1. The hydrogen and carbon atoms are shown by light gray and gray color, while nitrogen atoms by blue, iodine atoms by purple and tin atoms by green. The perovskite clusters are composed of tin atoms and iodine atoms to form SnI_6 octahedron. Then, according to the principle that total charge is zero, four $CH_3NH_3^+$ are added, and the three hydrogen atoms of the amino terminals in the four $CH_3NH_3^+$ are relative to the three iodine atoms of the octahedron with certain symmetry.

3.2. Adsorption configuration and adsorption energy

Due to the numerous models of perovskite cluster adsorbing water molecules [54], some typical models were selected in this study. Fig. 2 shows optimized structures of the adsorption of n water molecules (n = 1, 2, 3) on $(CH_3NH_3)_4SnI_6$. (1-a) and (1-b) are the stable configurations of perovskite cluster after adsorbing one water molecule, (2-a) to (2-c) are the stable configurations of perovskite cluster after adsorbing two water molecules and (3-a) to (3-d) are the stable configurations of perovskite cluster after adsorbing three water molecules. Table 1 shows the adsorption energy and interaction situation of adsorption configurations.

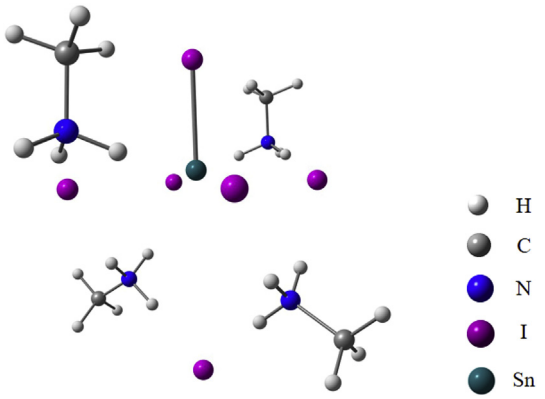

Fig. 1. Perovskite cluster model. (light gray, gray, blue, purple and green balls represent hydrogen, carbon, nitrogen, iodine and tin atoms). (For interpretation of the references to color in this figure legend, the reader is referred to the Web version of this article.)

Comparing with Fig. 1, the structure of perovskite cluster has changed a lot after the adsorption of water molecules. It can be seen from Table 1 that the absolute value of adsorption energy is between 41.71–55.60 kJ mol^{-1}. In configuration (1-a), the O atoms of the same water molecule exist interactions with two amino terminals of perovskite, and the absolute value of the adsorption energy is 55.26 kJ mol^{-1}. However, in configuration (1-b), water molecules interact with only one amino terminal, and the absolute value of adsorption energy is 48.57 kJ mol^{-1}. Thus, configuration (1-a) has stronger adsorption stability, and it shows that the adsorption stability is related to the number of interactions between water molecules and perovskite clusters.

The absolute value of adsorption energy of configuration (2-a) and configuration (2-c) is not significantly different, which is 53.48 kJ mol^{-1} and 51.18 kJ mol^{-1}, respectively. Configuration (2-b) is rather unstable and the absolute value of adsorption energy is relatively small, which is 41.71 kJ mol^{-1} (2-a) is formed on the basis of (1-a) that the water molecule is adsorbed on the original water molecule, and there are interactions between water molecules, forming small clusters and the adsorption is the most stable. While (2-b) and (2-c) is on the basis of (1-a) that the water molecule is adsorbed on one of the amino terminals, respectively. By comparing configuration (2-b) and (2-c), it can be found that (2-b) has one more such interaction than (2-c), but the absolute value of adsorption energy of configuration (2-b) is lower than that of configuration (2-a) and configuration (2-c), the specific reasons are given below.

Configuration (3-a) is based on configuration (2-a), and a water molecule is inserted between the amino terminal and water molecules. The absolute value of adsorption energy is 55.60 kJ mol^{-1}, and it is the most stable structure. Configuration (3-b) is based on configuration (2-a), in which water molecules are adsorbed on another amino terminal, and the absolute value of adsorption energy is 42.16 kJ mol^{-1}. Configuration (3-c) is based on configuration (2-a), in which the water molecule are directly adsorbed on water molecules to form small clusters without forming closed-loop, and the absolute value of adsorption energy is 48.84 kJ mol^{-1}. Configuration (3-d) is based on configuration (2-a) that two water molecules and one amino terminal form a closed loop as the new water molecule is adsorbed on another amino. The absolute value of absorption energy is slightly lower than configuration (3-a), which is 52.63 kJ mol^{-1}. This indicates that water on perovskite surface is not easy to form clusters entirely by water molecules, but easy to form closed-loop by water molecules and amino terminals.

According to the simple analysis above, it can be found that the adsorption energy is not only related to the interaction number, but also related to the interaction type. In this work, interaction types are divided into three categories: an amino terminal with a water molecule, water molecules, two amino terminals with the same water molecule.

By comparing configuration (2-a) with (2-c), it can be seen that the interaction between water molecules is much the same as the interaction between an amino and a water molecule. Back to the above problem that configuration (2-b) has one more interaction than (2-c) but the adsorption energy is lower, this is due to (2-b) has one more interaction between two amino terminals and a water molecule than (2-c), and it has one less interaction between an amino terminal and a water molecule. That is to say, at this point the interaction type has larger impacts than the interaction number. Comparing with configuration (3-a), there are two amino terminals interacting with the same

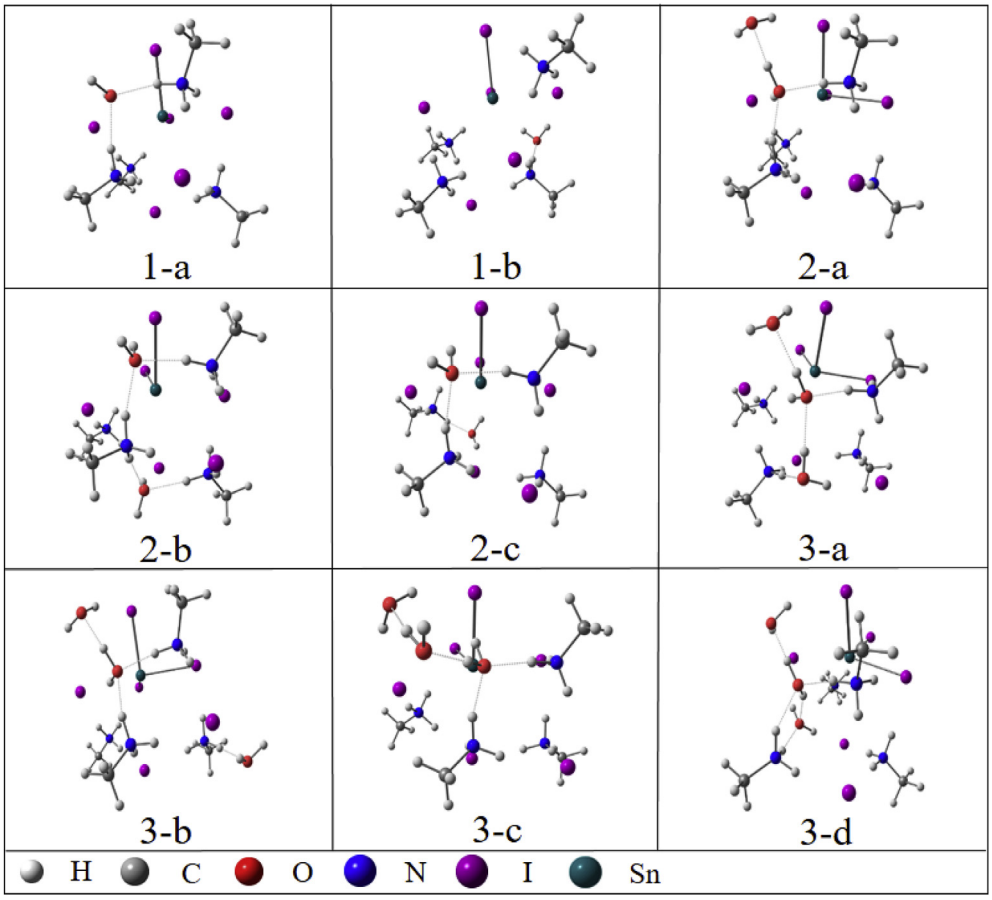

Fig. 2. Optimized structures of the adsorption of n water molecules (n = 1, 2, 3) on $(CH_3NH_3)_4SnI_6$.

Table 1
Adsorption energy and interaction of the adsorption configurations.

Configurations	E_{ads} (kJ mol^{-1})	Interaction number	Interaction type		
			1 amino, 1 water	1 water, 1 water	2 amino, 1 water
1-a	−55.26	2	0	0	1
1-b	−48.57	1	1	0	0
2-a	−53.48	3	0	1	1
2-b	−41.71	4	0	0	2
2-c	−51.18	3	1	0	1
3-a	−55.60	4	2	2	0
3-b	−42.16	4	1	1	1
3-c	−48.84	4	0	2	1
3-d	−52.63	4	0	2	1

water molecule in (3-b) and (3-c), and the absolute value of adsorption energy is lower. Therefore, it can be inferred that the interaction between two amino terminals and the same water molecule is weaker than that between one amino terminal and one water molecule or between two water molecules.

In conclusion, the stability of perovskite clusters after adsorbing less water molecules is related to the number and type of interactions. The interaction between an amino terminal and a water molecule or between two water molecules is almost the same, which is stronger than the interaction between two amino terminals and the same water molecule. When perovskite cluster adsorbs several water molecules, it tends to form a ring structure composed by amino terminals and water molecules.

3.3. IGM analysis

In 2010, Yang Weitao's team [55] proposed a reduced density gradient function (RDG) analysis method to analyze weak interactions in the system, including van der Waals interaction and hydrogen bond. This method is efficient and applicable to large systems, such as proteins or DNA [55]. However, this method is arbitrary for the selection of isosurface, and ignores the lattice points of some interaction regions [56].

In 2017, Corentin Lefebvre [56] and others proposed a new model which was the independent gradient model (IGM). Generally, when calculating the gradient of initial molecular density, the density gradient of each atom is simply added up, while the density gradient of IGM type is adding up the absolute value of each atoms' density gradient, and the two are subtracted to get the δ_g function, showing as follows:

$$\delta_g(r) = \left| \sum_i abs[\nabla \rho_i(r)] \right| - \sum_i \nabla \rho_i(r) \tag{3}$$

where $\nabla \rho_r$ represents the electronic density gradient and i represents the atomic serial number.

The intensity and type of weak interaction can be visually reflected by projecting the electron density $\rho(r)$ and the corresponding $\text{sign}(\lambda_2)$ function values (symbolic function, λ_2 is the second eigenvalue of Hessian matrix of electron density ρ) on the isosurface of the δ_g function. Using this model can conveniently investigate the weak interaction between inter-fragment or intra-fragment in molecular, and overcome the inconvenience caused by the reduced density gradient function method [57], so that the final isosurface map is able to be more accurate and full.

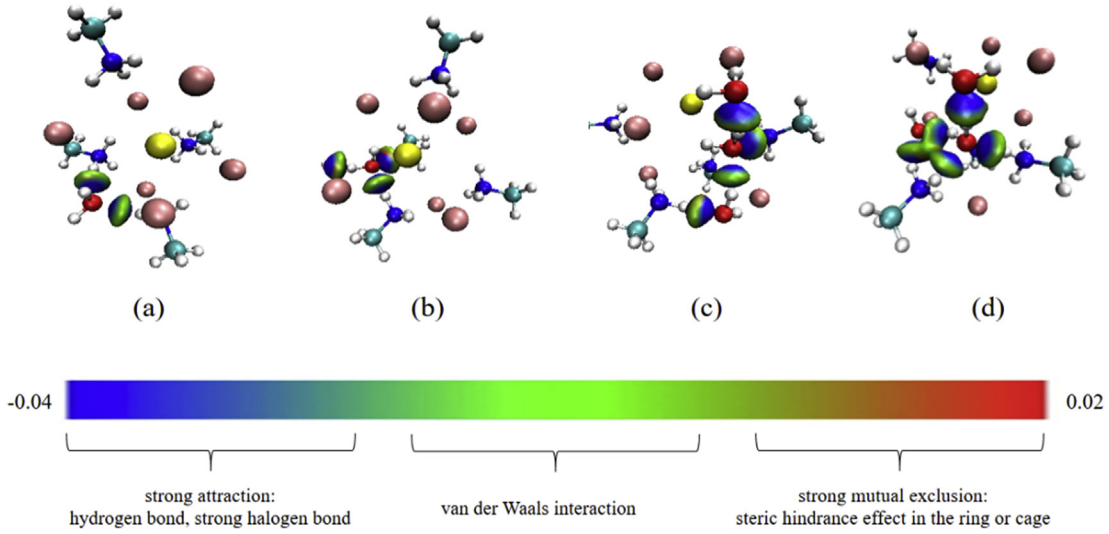

Fig. 3. The IGM isosurface color maps of the four adsorption configurations (a) 1-a, (b) 2-a, (c) 3-a, (d) 3-d. (For interpretation of the references to color in this figure legend, the reader is referred to the Web version of this article.)

The weak interaction between molecules can be visually seen from the IGM isosurface color map. The location of interaction between molecules can be judged according to the space position filled with the isosurface. The type and relative intensity of interaction can be judged according to the color of the isosurface. In this work, in order to better explain the positions and types of molecular interactions, the stable adsorption configurations with the largest interaction energy among each category were selected, respectively. Thus, adsorption configurations (1-a), (2-a), (3-a) and (3-d) were chosen as the research objects, and the corresponding RDG isosurface color maps are shown in Fig. 3. In the isograms, the dark blue region has strong attraction, which is generally hydrogen bond and strong halogen bond and so on; the green region has weak attraction, which is van der Waals interaction; the red region shows strong mutual exclusion, which is generally the steric hindrance effect in the ring or cage.

It can be seen from Fig. 3 that there are mainly blue isosurface between water molecules and the amino terminals of the perovskite cluster, and the same thing happens between the water molecules, while the edge is green isosurface. It indicates that the attraction between water molecules and the perovskite cluster is mainly hydrogen bond. In Fig. 3(b), when two water molecules are adsorbed on the perovskite molecular surface, there are still a few red isosurface on the water molecule and two amino terminals of the perovskite cluster, indicating that there is also steric hindrance between water molecules and the perovskite cluster. As can be seen from Fig. 3(d), in the configuration (3-d), the amino terminal of the perovskite cluster model forms a ternary ring with two water molecules by hydrogen bonds. In conclusion, the adsorption of water molecules on the surface of the perovskite cluster model is all achieved by hydrogen bonds, and there is a weak van der Waals interaction. So the adsorption stability is weak, which is consistent with the result that the adsorption energy is small in the previous calculation.

3.4. AIM analysis

Bader et al. [58] proposed the theory of atoms in molecules (AIM) in the 1960 s, Carrol and Bader [59,60] proposed that when $\nabla^2\rho(r) > 0$, the interaction type is non covalent bond such as hydrogen bond and halogen bond, and when $\nabla^2\rho(r) < 0$, the interaction type is considered as covalent bond. In addition, Espinoza [61] proposed to judge the interaction type based on the relationship among the potential energy density $V(r)$, Laplace energy density $G(r)$ and the total energy density $H(r)$ at the critical point of the bond. When $|V(r)|/G(r) > 2$, the interaction is covalent bond, while it is non covalent bond when $|V(r)|/G(r) < 2$.

The interaction path among interacting atoms between the perovskite clusters and water molecules can be obtained by AIM topological analysis of adsorption configuration [62]. According to the topological parameters of the bond critical points (BCPs) in the interaction path, the interaction types between atoms can be more accurately judged and the strength of different types of interaction can be quantitatively compared [63]. In this work, in order to better understand the interaction paths, the most stable adsorption configurations with the largest interaction energy among each category were selected, respectively. Thus, adsorption configurations (1-a), (2-a), (2-c) and (3-a) were chosen as the research objects. The AIM topological paths of the

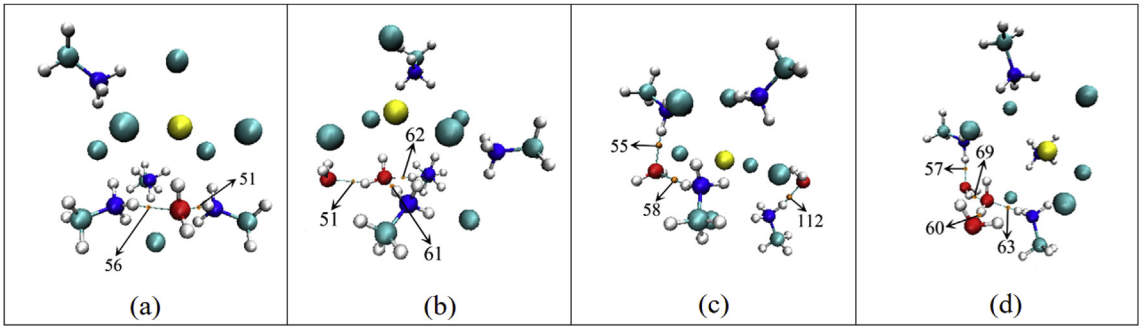

Fig. 4. The AIM topological path maps of the four configurations (a) 1-a, (b) 2-a, (c) 2-c, (d) 3-a.

Table 2
Topological parameters of the BCPs in the adsorption configurations.

Configures	N	ρ	$\nabla^2\rho$	G(r)	V(r)	|V(r)|/G(r)	H(r)	δ_g(r)	Length (nm)
1-a	51	0.0254	0.0833	0.0194	−0.0181	0.9330	0.0014	0.0450	0.1963
	56	0.0246	0.0810	0.0188	−0.0174	0.9255	0.0014	0.0443	0.1977
2-a	51	0.0404	0.1011	0.0307	−0.0361	1.1759	0.0054	0.0701	0.1783
	61	0.0348	0.0981	0.0264	−0.0283	1.0720	0.0019	0.0612	0.1840
	62	0.0348	0.1061	0.0279	−0.0294	1.0538	0.0014	0.0675	0.1822
2-c	55	0.0265	0.0203	0.0203	−0.0193	0.9507	0.0010	0.0478	0.1943
	58	0.0248	0.0191	0.0191	−0.0175	0.9162	0.0015	0.0440	0.1975
	112	0.0469	0.1071	0.0348	−0.0429	1.2328	0.0081	0.0812	0.1729
3-a	57	0.0271	0.0877	0.0214	−0.0209	0.9766	0.0005	0.0496	0.1927
	60	0.0426	0.1025	0.0323	−0.0390	1.2074	0.0067	0.0740	0.1757
	63	0.0376	0.1022	0.0286	−0.0317	1.1084	0.0031	0.0661	0.1807
	69	0.0543	0.1136	0.0404	−0.0524	1.2970	0.0120	0.0941	0.1663

adsorption configuration are shown in Fig. 4, and the parameters of BCPs in the topological paths are shown in Table 2.

As shown in Fig. 4, in the above models, there exists topological paths between O atoms of the water molecule and H atoms of two amino terminals in the perovskite cluster or between two water molecules, and the BCPs are found in the path, showing that there is interaction between the water molecule and two amino terminals of the perovskite cluster or between two water molecules. As shown in Table 2, it can be found that the Laplace value of electron density at BCPs is greater than zero, indicating that the interaction corresponding to the critical point belongs to closed-shell interplay. In addition, according to Espinoza's criterion, the topological parameters at BCPs adjust to $|V(r)|/G(r) < 2$, indicating that the above interaction types are non-covalent bond.

In configuration (1-a), the electron densities ρ of the two bond critical points is 0.0254 and 0.0246, the δ_g values are 0.0450 and 0.0443, and the total potential energy densities are both 0.0014, indicating that the hydrogen bond strength of the two bonds is almost the same. The lengths of the two hydrogen bonds are 0.1963 nm and 0.1977 nm, respectively, proving that the two bonds are as strong as each other. In configuration (2-a), the electron density ρ, the total potential energy density H and δ_g at the BCP (No. 51) between the two water molecules are all larger than the BCPs (No. 61, 62) between the water molecule and the two amino terminals. The hydrogen bond length between the two water molecules is the shortest, which is 0.1783 nm, showing that the interaction strength in water molecules is larger than that between a water molecule and two amino terminals. This is consistent with the conclusion obtained from comparing the adsorption energy in the above study. Similarly, in configuration (2-c), the electron density ρ, the total potential energy density H and δ_g at the BCP (No. 112) between one amino terminal and one water molecule is all larger than that (No. 55, 58) between the water molecule and two amino terminals. The hydrogen bond length between one amino terminal and one water molecule is also the shortest, which is 0.1729 nm, showing that the interaction strength in one amino and one water molecule is larger than that between a water molecule and two amino terminals. This is consistent with the conclusion obtained from comparing the adsorption energy in the above study. In configuration (3-a), there is only interactions between water molecules (No. 60, 69) or between a water molecule and an amino terminal (No. 57, 63). Through the comparison of ρ, H, δ_g and the size of hydrogen bonds, it can be seen that interaction intensity between water molecules is a bit stronger than that between a water molecule and an amino terminal.

In conclusion, AIM analysis was conducted on the adsorption configuration of water molecules at the surface of the perovskite cluster model to obtain the specific interaction path between the molecules. According to the topological parameters of the BCPs, it could be obtained that water molecules are all adsorbed on the surface of the perovskite cluster model by hydrogen bonds. The strength of different interaction types were compared by topological parameters and the conclusion is basically consistent with that obtained from adsorption energy analysis above.

4. Conclusion

In this work, the adsorption mechanism of single and multiple water molecules on the surface of perovskite cluster model was studied by density functional theory. Through adsorption energy calculation, IGM and AIM analysis of various optimized adsorption configurations, the conclusions are as follows:

1 The interactions between an amino terminal and a water molecule or between two water molecules were both stronger than that between two amino terminals and the same water molecule.
2 When perovskite cluster adsorbed multiple water molecules, it was easier to form a ring structure composed of amino terminals and water molecules.
3 The interactions between water molecules and perovskite cluster were visually shown by IGM analysis that the interaction belonged to hydrogen bond and Van der Waals interaction exists.
4 The interaction paths and types were visually displayed through AIM topological analysis which revealed that water molecules were all adsorbed on the perovskite cluster by hydrogen bonds.
5 Cluster size, inorganic element or organic element can be adjusted to study the composition effect. The stability of hybrid perovskite can be improved by adjusting the composition of perovskite materials and finding suitable combinations.

Acknowledgements

This work was supported by the Beijing Municipal Natural Science Foundation (2182066), Natural Science Foundation of Hebei Province of China (B2018502067) and the Fundamental Research Funds for the Central Universities (JB2015RCY03 and 2017XS121). Computational resources from TianHe-2 at Lvliang Supercomputer Center were acknowledged.

Appendix A. Supplementary data

Supplementary data to this article can be found online at https://doi.org/10.1016/j.solmat.2019.110126.

References

[1] A. Kojima, K. Teshima, Y. Shirai, T. Miyasaka, Organometal halide perovskites as visible-light sensitizers for photovoltaic cells, J. Am. Chem. Soc. 131 (2009) 6050–6051.
[2] American Association for the Advancement of Science, Newcomer juices up the race to harness sunlight, Science (2013).
[3] N.-G. Park, Perovskite solar cells: an emerging photovoltaic technology, Mater. Today 18 (2015) 65–72.
[4] H.J. Queisser, Slip patterns on boron-doped silicon surfaces, J. Appl. Phys. 32

(1961) 1776–1780.
[5] L.G. Gerling, S. Mahato, A. Morales-Vilches, G. Masmitja, P. Ortega, C. Voz, R. Alcubilla, J. Puigdollers, Transition metal oxides as hole-selective contacts in silicon heterojunctions solar cells, Sol. Energy Mater. Sol. Cells 145 (2016) 109–115.
[6] T. Baikie, Y. Fang, J.M. Kadro, M. Schreyer, F. Wei, S.G. Mhaisalkar, M. Graetzel, T.J. White, Synthesis and crystal chemistry of the hybrid perovskite (CH_3 NH_3) PbI_3 for solid-state sensitised solar cell applications, J. Mater. Chem. 1 (2013) 5628–5641.
[7] J.E. Spanier, V.M. Fridkin, A.M. Rappe, A.R. Akbashev, A. Polemi, Y. Qi, Z. Gu, S.M. Young, C.J. Hawley, D. Imbrenda, Power conversion efficiency exceeding the shockley–queisser limit in a ferroelectric insulator, Nat. Photonics vol 10, (2016) 611.
[8] C. Sun, F. Pan, H. Bin, J. Zhang, L. Xue, B. Qiu, Z. Wei, Z.-G. Zhang, Y. Li, A low cost and high performance polymer donor material for polymer solar cells, Nat. Commun. 9 (2018) 743.
[9] J.H. Im, C.R. Lee, J.W. Lee, S.W. Park, N.G. Park, 6.5% efficient perovskite quantum-dot-sensitized solar cell, Nanoscale 3 (2011) 4088–4093.
[10] N.-G. Park, Organometal perovskite light absorbers toward a 20% efficiency low-cost solid-state mesoscopic solar cell, J. Phys. Chem. Lett. 4 (2013) 2423–2429.
[11] C. Re, G. Uerr, Perovskite solar cells keep on surging, Science 344 (2014) 458-458.
[12] N.J. Jeon, H. Na, E.H. Jung, T.-Y. Yang, Y.G. Lee, G. Kim, H.-W. Shin, S. Il Seok, J. Lee, J. Seo, A fluorene-terminated hole-transporting material for highly efficient and stable perovskite solar cells, Nat. Energy 3 (2018) 682–689.
[13] Best Research-Cell Efficiency Chart, (2019).
[14] A decade of perovskite photovoltaics, Nat. Energy 4 (2019) 1 1.
[15] M. Petrović, V. Chellappan, S. Ramakrishna, Perovskites: solar cells & engineering applications–materials and device developments, Sol. Energy 122 (2015) 678–699.
[16] G. Niu, X. Guo, L. Wang, Review of recent progress in chemical stability of perovskite solar cells, J. Mater. Chem. vol 3, (2015) 8970–8980.
[17] M. Shahbazi, H. Wang, Progress in research on the stability of organometal perovskite solar cells, Sol. Energy 123 (2016) 74–87.
[18] S. De Wolf, J. Holovsky, S.-J. Moon, P. Löper, B. Niesen, M. Ledinsky, F.-J. Haug, J.-H. Yum, C. Ballif, Organometallic halide perovskites: sharp optical absorption edge and its relation to photovoltaic performance, J. Phys. Chem. Lett. vol 5, (2014) 1035–1039.
[19] J.M. Frost, K.T. Butler, F. Brivio, C.H. Hendon, M. van Schilfgaarde, A. Walsh, Atomistic origins of high-performance in hybrid halide perovskite solar cells, Nano Lett. 14 (2014) 2584–2590.
[20] Q.L. Jiang, D. Rebollar, J. Gong, E.L. Piacentino, C. Zheng, T. Xu, Pseudohalide-induced moisture tolerance in perovskite CH3NH3Pb(SCN)(2)I thin films, Angew. Chem. Int. Ed. 54 (2015) 7617–7620.
[21] U. Kreibig, M. Vollmer, Optical Properties of Metal Clusters, Springer Science & Business Media, 2013.
[22] L. Li, Y. Chen, Z. Liu, Q. Chen, X. Wang, H.J.A.m. Zhou, The additive coordination effect on hybrids perovskite crystallization and high-performance, Sol. Cells 28 (2016) 9862–9868.
[23] J.W. McFarland, D.J. Gans, Cluster significance analysis contrasted with three other quantitative structure-activity relationship methods, J. Med. Chem. 30 (1987) 46–49.
[24] H. Fang, P. Jena, Molecular origin of properties of organic–inorganic hybrid perovskites: the big picture from small clusters, J. Phys. Chem. Lett. vol 7, (2016) 1596–1603.
[25] G. Pacchioni, P.S. Bagus, F. Parmigiani, Cluster Models for Surface and Bulk Phenomena, Springer Science & Business Media, 2013.
[26] G. Giorgi, T. Yoshihara, K. Yamashita, Structural and electronic features of small hybrid organic-inorganic halide perovskite clusters: a theoretical analysis, Phys. Chem. Chem. Phys. 18 (2016) 27124–27132.
[27] G. Giorgi, K. Yamashita, Zero-dimensional hybrid organic–inorganic halide perovskite modeling: insights from first principles, J. Phys. Chem. Lett. vol 7, (2016) 888–899.
[28] T.J. Huang, Z.X. Thiang, X. Yin, C. Tang, G. Qi, H. Gong, (CH3NH3) 2PdCl4: a compound with two-dimensional organic–inorganic layered perovskite structure, Chem. Eur J. 22 (2016) 2146–2152.
[29] C. Kagan, D. Mitzi, C. Dimitrakopoulos, Organic-inorganic hybrid materials as semiconducting channels in thin-film field-effect transistors, Science vol 286, (1999) 945–947.
[30] J.L. Knutson, J.D. Martin, D.B. Mitzi, Tuning the Band Gap In Hybrid Tin Iodide Perovskite Semiconductors Using Structural Templating, Inorg. Chem. vol 44, (2005) 4699–4705.
[31] L. Ma, J. Dai, X.C. Zeng, Two-dimensional single-layer organic-inorganic hybrid perovskite semiconductors, Adv. Energy Mater. 7 (2017) 1601731.
[32] X. Zhang, X. Ren, B. Liu, R. Munir, X. Zhu, D. Yang, J. Li, Y. Liu, D.-M. Smilgies, R. Li, Stable high efficiency two-dimensional perovskite solar cells via cesium doping, Energy Environ. Sci. vol 10, (2017) 2095–2102.
[33] G. Giorgi, K. Yamashita, Organic-inorganic halide perovskites: an ambipolar class of materials with enhanced photovoltaic performances, J. Mater. Chem. 3 (2015) 8981–8991.
[34] Z. Gao, Y. Ding, W. Yang, W. Han, DFT study of water adsorption on lignite molecule surface, J. Mol. Model. 23 (2017) 27.
[35] F. Neese, The ORCA program system, Wiley Interdiscip. Rev., Comput. Mol. Sci. 2 (2012) 73–78.
[36] P. Stephens, F. Devlin, C. Chabalowski, M.J. Frisch, Ab initio calculation of vibrational absorption and circular dichroism spectra using density functional force fields, J. Phys. Chem. vol 98, (1994) 11623–11627.
[37] F. Weigend, R. Ahlrichs, Balanced basis sets of split valence, triple zeta valence and quadruple zeta valence quality for H to Rn: design and assessment of accuracy, Phys. Chem. Chem. Phys. 7 (2005) 3297–3305.
[38] S. Grimme, S. Ehrlich, L. Goerigk, Effect of the damping function in dispersion corrected density functional theory, J. Comput. Chem. 32 (2011) 1456–1465.
[39] H. Kruse, S. Grimme, A geometrical correction for the inter-and intra-molecular basis set superposition error in hartree-fock and density functional theory calculations for large systems, J. Chem. Phys. vol 136, (2012) 04B613.
[40] F. Sagan, R. Filas, M. Mitoraj, Non-covalent interactions in hydrogen storage materials $LiN(CH_3)_2BH_3$ and $KN(CH_3)_2BH_3$, Crystals (2016) 6.
[41] N.-X. Qiu, Y. Xue, Y. Guo, W.-J. Sun, W. Chu, Adsorption of methane on carbon models of coal surface studied by the density functional theory including dispersion correction (DFT-D3), Comput. Theor. Chem. 992 (2012) 37–47.
[42] W. Gao, H. Feng, X. Xuan, L. Chen, The assessment and application of an approach to noncovalent interactions: the energy decomposition analysis (EDA) in combination with DFT of revised dispersion correction (DFT-D3) with Slater-type orbital (STO) basis set, J. Mol. Model. 18 (2012) 4577–4589.
[43] T. van der Wijst, C. Fonseca Guerra, M. Swart, F.M. Bickelhaupt, B. Lippert, A ditopic ion-pair receptor based on stacked nucleobase quartets, Angew Chem. Int. Ed. Engl. 48 (2009) 3285–3287.
[44] C. Fonseca Guerra, T. van der Wijst, J. Poater, M. Swart, F.M. Bickelhaupt, Adenine versus guanine quartets in aqueous solution: dispersion-corrected DFT study on the differences in π-stacking and hydrogen-bonding behavior, Theor. Chem. Acc. 125 (2009) 245–252.
[45] J. Witte, J.B. Neaton, M. Head-Gordon, Effective empirical corrections for basis set superposition error in the def2-SVPD basis: gCP and DFT-C, J. Chem. Phys. 146 (2017) 234105.
[46] F. Weigend, A fully direct RI-HF algorithm: implementation, optimised auxiliary basis sets, demonstration of accuracy and efficiency, Phys. Chem. Chem. Phys. 4 (2002) 4285–4291.
[47] L. Goerigk, S. Grimme, A thorough benchmark of density functional methods for general main group thermochemistry, kinetics, and noncovalent interactions, Phys. Chem. Chem. Phys. 13 (2011) 6670–6688.
[48] T. Lu, F. Chen, Multiwfn: a multifunctional wavefunction analyzer, J. Comput. Chem. 33 (2012) 580–592.
[49] W. Humphrey, A. Dalke, K. Schulten, VMD: visual molecular dynamics, J. Mol. Graph. 14 (1996) 33–38.
[50] W.D. Arnold, E. Oldfield, The chemical nature of hydrogen bonding in proteins via NMR: J-couplings, chemical shifts, and AIM theory, J. Am. Chem. Soc. 122 (2000) 12835–12841.
[51] J. Chen, X. Long, Y. Chen, Comparison of multilayer water adsorption on the hydrophobic galena (PbS) and hydrophilic pyrite (FeS_2) surfaces: a DFT study, J. Phys. Chem. 118 (2014) 11657–11665.
[52] Z. Gao, X. Liu, A. Li, C. Ma, X. Li, X. Ding, W. Yang, Adsorption behavior of mercuric oxide clusters on activated carbon and the effect of SO_2 on this adsorption: a theoretical investigation, J. Mol. Model. 25 (2019) 142.
[53] V.M. Goldschmidt, Die gesetze der krystallochemie, 14 (1926) 477–485.
[54] J. Kowalski, K. Johnson, H. Tuller, Models for the photoelectrolytic decomposition of water at semiconducting oxide anodes, J. Electrochem. Soc. vol 127, (1980) 1969–1973.
[55] E.R. Johnson, S. Keinan, P. Mori-Sanchez, J. Contreras-García, A.J. Cohen, W. Yang, Revealing noncovalent interactions, J. Am. Chem. Soc. 132 (2010) 6498–6506.
[56] C. Lefebvre, G. Rubez, H. Khartabil, J.C. Boisson, J. Contreras-Garcia, E. Henon, IGM, Phys. Chem. Chem. Phys. 19 (2017) 17928–17936.
[57] G. Saleh, C. Gatti, L.L. Presti, Non-covalent interaction via the reduced density gradient: independent atom model vs experimental multipolar electron densities, Comput. Theor. Chem. 998 (2012) 148–163.
[58] R.F.W. Bader, Atoms in molecules, Acc. Chem. Res. 18 (1985) 9–15.
[59] M.T. Carroll, R.F.W. Bader, An analysis of the hydrogen bond in base-hf complexes using the theory of atoms in molecules, Mol. Phys. vol 65, (1988) 695–722.
[60] M.T. Carroll, C. Chang, R.F.W. Bader, Prediction of the structures of hydrogen-bonded complexes using the laplacian of the charge density, Mol. Phys. 63 (1988) 387–405.
[61] E. Espinosa, I. Alkorta, J. Elguero, E. Molins, From weak to strong interactions: a comprehensive analysis of the topological and energetic properties of the electron density distribution involving X–H···F–Y systems, J. Chem. Phys. 117 (2002) 5529–5542.
[62] C. Wu, A. De Visscher, I.D. Gates, Molecular interactions between 1-butyl-3-methylimidazolium tetrafluoroborate and model naphthenic acids: a DFT study, J. Mol. Liq. 243 (2017) 462–471.
[63] Z. Gao, Y. Ding, DFT study of CO_2 and H_2O co-adsorption on carbon models of coal surface, J. Mol. Model. 23 (2017) 187.